AIMS Mathematics, 9(2): 4781–4804.
DOI: 10.3934/math.2024231
Received: 09 November 2023
Revised: 26 December 2023
Accepted: 11 January 2024
Published: 22 January 2024

http://www.aimspress.com/journal/Math

Research article

A state-dependent impulsive system with ratio-dependent action threshold for investigating SIR model

Yongfeng Li[1,*], **Song Huang**[1] **and Zhongyi Xiang**[2]

[1] Department of Mathematics and Information Science, Zhengzhou University of Light Industry, Zhengzhou 450002, China

[2] School of Mathematics and Statistics, Hubei Minzu University, Enshi 445000, China

* **Correspondence:** Email: yfli2003@163.com.

Abstract: In general, there is an imperative to amalgamate timely interventions and comprehensive measures for the efficacious control of infectious diseases. The deployment of such measures is intricately tied to the system's state and its transmission rate, presenting formidable challenges for stability and bifurcation analyses. In our pursuit of devising qualitative techniques for infectious disease analysis, we introduced a model that incorporates state-dependent transmission interventions. Through the introduction of state-dependent control, characterized by a non-linear action threshold contingent upon the combination of susceptible population density and its rate of change, we employ analytical methods to scrutinize various facets of the model. This encompasses addressing the existence, stability, and bifurcation phenomena concerning disease-free periodic solutions (DFPS). The analysis of the established Poincaré map leads us to the conclusion that DFPS indeed exists and maintains stability under specific conditions. Significantly, we have formulated a distinctive single-parameter family of discrete mappings, leveraging the bifurcation theorems of discrete maps to dissect the transcritical bifurcations around DFPS with respect to parameters such as ET and η_1. Under particular conditions, these phenomena may give rise to effects like backward bifurcation and bistability. Through the analytical methodologies developed in this study, our objective is to unveil a more comprehensive understanding of infectious disease models and their potential relevance across diverse domains.

Keywords: impulsive control; action threshold; Poincaré map; transcritical bifurcation; periodic solutions
Mathematics Subject Classification: 37N25, 93C27

1. Introduction

Infectious diseases have consistently posed a significant challenge to public health globally. Historically, pandemics such as the plague, black death, and the 1918 Spanish influenza have led to the loss of millions, even tens of millions, deeply affecting the political, social, and economic structures of societies. Today, despite major advancements in medical and healthcare sciences, outbreaks like SARS, H1N1, Ebola, and COVID-19 continue to threaten global health.

In the fight against infectious diseases, mathematical modeling has become an indispensable tool, offering insights into the study, understanding, and management of disease spread [1–10]. By establishing appropriate mathematical models, we can analyze the effectiveness of control measures quantitatively or qualitatively. Among these models, the state-dependent pulse model is particularly noteworthy for its ability to effectively describe infectious disease control [11, 12]. The model operates under the assumption that no control measures are implemented when the number of susceptible populations is within a certain range. However, comprehensive measures, including immunization of susceptible populations and treatment of infected individuals, are implemented when the size of the susceptible population reaches or exceeds the control threshold. Subsequently, scholars have developed numerous state-dependent pulse models tailored to different types of infectious disease characteristics, delving into the impact of state-dependent pulse control strategies on dynamic behaviors, such as disease elimination and epidemics.

Nevertheless, many existing mathematical models of infectious diseases assume continuous interventions like vaccination, drug treatment, or isolation. These models frequently overlook real-world challenges, including resource constraints, high costs, and the impracticality of sustained interventions. Addressing these issues, pulse control strategies, involving periodic interventions like vaccination or patient isolation, have garnered significant attention in the field of mathematical modeling. Pulse control proves particularly beneficial in resource-limited scenarios and is extensively researched for its potential in infectious disease control [13–20]. Furthermore, state-dependent feedback control, as represented by pulse semi-dynamic systems, finds application across various fields and sciences, such as fisheries harvesting [21–23], integrated pest management [24–26], and interactions among biological populations [27–29].

In the realm of infectious disease modeling, the selection of the ratio-dependent action threshold method is driven by a meticulous consideration of the limitations inherent in traditional control strategies and the imperative need for a more realistic representation of disease dynamics. The foundational premise of triggering interventions based on a fixed population density threshold, a cornerstone of state-dependent feedback control, tends to oversimplify the intricate dynamics of real-world scenarios. This conventional approach may overlook crucial factors, such as situations where the transmission rate remains high despite a low population density or vice versa. In both scenarios, a high population density may not necessarily warrant immediate control intervention if the transmission rate remains low. To address this limitation, the adoption of a more effective control strategy becomes imperative. This strategy considers both population density and its rate of change, leading to the formulation of a nonlinear threshold control policy known as the "ratio-dependent action threshold". In this approach, the decision to implement control measures hinges on the ratio of population density to its rate of change, providing a more adaptive and realistic representation of infectious disease scenarios.

The significance of the ratio-dependent action threshold method lies in its capacity to capture the nuanced dynamics of infectious diseases. Recent research has delved into nonlinear threshold strategies, revealing diverse and dynamic behaviors in various contexts [30–36]. This method not only challenges prevailing assumptions in pulse control models, where the rate of change is assumed to directly correlate with population density following the introduction of control measures but also offers a more accurate representation by acknowledging inherent constraints in this relationship. Furthermore, the adoption of a saturated form that includes a nonlinear function enhances the realism of infectious disease models. This nuanced approach considers the complexities of disease dynamics, contributing to a more comprehensive understanding of infectious diseases and facilitating the development of intervention strategies aligned with the dynamic nature of disease transmission. In summary, the ratio-dependent action threshold method is chosen for its ability to address real-world complexities, offering a more accurate and adaptive representation of infectious disease dynamics in modeling and control strategies.

Our efforts aim to integrate a nonlinear threshold strategy within an infectious disease transmission model with a saturated incidence rate. In Section 2, we introduce an SIR state-dependent pulse model with a saturated incidence rate and adopt a rate-related nonlinear action threshold. Section 3 delves into constructing the corresponding Poincaré map by defining the pulse set and phase set range and discussing the essential attributes of the Poincaré map. In Section 4, conditions for the existence and stability of 1st order periodic solutions are established. Section 5 analyzes the bifurcation of the discrete mapping's one-parameter family concerning a critical parameter near the trivial fixed point when the model possesses a local disease equilibrium. Sensitivity analysis of the model is conducted in Section 6, where variations in parameters lead to complex dynamics. The analysis of the intricate interplay remains a challenging and underexplored frontier in this domain. Finally, a comprehensive conclusion and detailed discussions wrap up our study.

2. Model

In our current study, we have chosen an SIR model with a saturated incidence rate, and extended the model presented in [37] by considering the density of susceptible individuals and their rate of change as action thresholds. The model is given by the following equation:

$$\begin{cases} \left.\begin{aligned} \frac{dS(t)}{dt} &= \Lambda - \frac{\beta S I}{1+\alpha S} - \delta S, \\ \frac{dI(t)}{dt} &= \frac{\beta S I}{1+\alpha S} - (\gamma+\delta) I, \end{aligned}\right\} & u_1 S(t) + v_1 \frac{dS(t)}{dt} < ET, \\ \left.\begin{aligned} S(t^+) &= (1-\eta_1) S(t), \\ I(t^+) &= (1-\eta_2) I(t), \end{aligned}\right\} & u_1 S(t) + v_1 \frac{dS(t)}{dt} = ET. \end{cases} \tag{1}$$

Here, $S(t)$ and $I(t)$ denote the numbers of susceptible and infected individuals, respectively. Λ is the birth rate, δ is the mortality rate, γ indicates the rate of recovery, β is the rate at which transmission occurs, and α is the half-saturation constant. Additionally, we define q as $q = \gamma + \delta$. The parameters u_1, v_1, and ET are all positive constants, and to simplify the model, we set $u_1 + v_1 = 1$. When the

population density of susceptible individuals reaches the action threshold given by

$$u_1 S(t) + v_1 \frac{dS(t)}{dt} = ET$$

control measures will be implemented to update the numbers of susceptible individuals and infected individuals as follows: $(1-\eta_1)S(t)$ and $(1-\eta_2)I(t)$. In this context, η_1 and η_2 represent the maximum vaccination rate and maximum treatment rate, respectively. The parameters u_1, v_1, ET, η_1, and η_2 are pivotal factors within the control of decision-makers, intricately associated with infectious disease control measures. The values of these parameters can be effectively determined through practical applications in the field of infectious disease control.

The dynamic analysis of the non-pulsed model in [37] has been extremely valuable for our research. We define the non-pulsed model as M_0, and, based on [37], it is evident that M_0 possesses a disease-free equilibrium point, denoted as $E_0(K, 0)$, where E_0 is stable when $R_0 < 1$, and it becomes unstable when $R_0 > 1$, where

$$R_0 = \frac{\Lambda(\beta - \alpha q)}{\delta q}, \quad K = \frac{\Lambda}{\delta}.$$

Furthermore, M_0 has an endemic equilibrium point denoted as $E^*(S^*, I^*)$ for $R_0 > 1$, where

$$S^* = \frac{q}{\beta - \alpha q}, \quad I^* = \frac{\Lambda(\beta - \alpha q) - \delta q}{q(\beta - \alpha q)}.$$

In cases where $\Delta \geq 0$, $E(S, I^*)$ is a stable node, while for $\Delta < 0$, it behaves as a stable focus, where

$$\Delta = \frac{\delta^2(\beta - \alpha q)^2(R_0 - 1)^2}{\beta^2} + \frac{\delta(2\delta - 4q)(\beta - \alpha q)(R_0 - 1)}{\beta} + \delta^2.$$

It follows from

$$u_1 S(t) + v_1 \frac{dS(t)}{dt} = ET$$

that we have

$$u_1 S + v_1\left(\Lambda - \frac{\beta S I}{1 + \alpha S} - \delta S\right) = ET,$$

and we can define the impulsive curve as

$$L_M : I = \frac{(u_1 S + v_1(\Lambda - \delta S) - ET)(1 + \alpha S)}{v_1 \beta S}.$$

Since

$$S(t^+) = (1-\eta_1)S(t) \text{ and } I(t^+) = (1-\eta_2)I(t),$$

we can define the corresponding phase space as

$$L_N : I = (1-\eta_2)L_M\left(\frac{S}{1-\eta_1}\right).$$

According to $\frac{dS}{dt} = 0$, we can denote the vertical isocline as

$$L_1 : I = \frac{(\Lambda - \delta S)(1 + \alpha S)}{\beta S}.$$

There is an intersection point between L_1 and L_M for

$$L_M(S) - L_1(S) = 0,$$

where

$$L_M = L_1 + \frac{(u_1 S - ET)(1 + \alpha S)}{v_1 \beta S},$$

and the intersection point denote as

$$P_{ET} = (S_{ET}, I_{ET}),$$

where

$$S_{ET} = \frac{ET}{u_1}$$

and

$$I_{ET} = \frac{(\Lambda u_1 - \delta ET)(u_1 + \alpha ET)}{u_1 \beta ET}.$$

If $K > \frac{ET}{u_1}$, then there is a unique intersection P_{ET} where all coordinates are positive. However, when $u_1 = 0$, the inequality $L_M(S) < L_1(S)$ always holds, indicating that lines L_M and L_1 do not intersect.

3. Poincaré map for $R_0 < 1$

The trajectory starting from any point $P_k^+ = (S_k^+, I_k^+)$ on L_N will definitely reach L_M after finite time t, and its intersection with L_M is

$$P_{k+1} = (S_{k+1}, I_{k+1}),$$

and it will pulse to point $P_{k+1}^+ \subset L_N$. Therefore, we can denote

$$P_{k+1}^+ = (S_{k+1}^+, I_{k+1}^+)$$

with

$$S_{k+1}^+ = (1 - \eta_1) S_{k+1}, \;\; I_{k+1}^+ = (1 - \eta_2) I_{k+1},$$

and we define the Poincaré map P_M as

$$P_M(I_k^+) = (1 - \eta_2) I_{k+1} = I_{k+1}^+.$$

There exists a point on L_N, denoted as $P_T = (S_T, I_T)$. The trajectory starting from P_T reaches L_M at point $P_{T1} = (S_{T1}, I_{T1})$ (see Figure 1). Therefore, we define the impulsive set and phase set as

$$M = \{(S, I) | S_Z \leq S \leq S_{T1,}, 0 \leq I \leq I_{T1}\},$$

$$N = \{(S^+, I^+) | S_Z^+ \leq S^+ \leq (1 - \eta_1) S_{T1}, 0 \leq I^+ \leq (1 - \eta_2) I_{T1}\}.$$

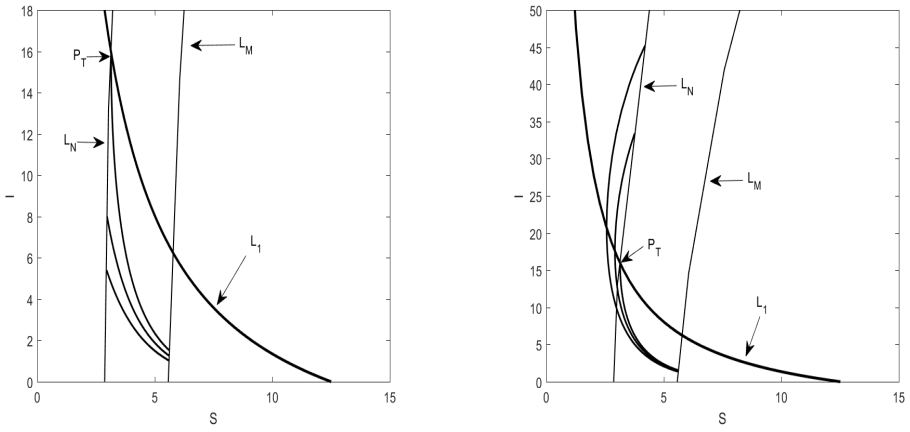

Figure 1. The trajectories of system (1) for $R_0 < 1$, where $\Lambda = 1$, $\beta = 0.015$, $\alpha = 0.001$, $\delta = 0.08$, $\gamma = 0.3$, $\eta_1 = 0.5$, $\eta_2 = 0.1$, $u_1 = 0.7$, $v_1 = 0.3$, and $ET = 4$.

We denote continuous functions $Q_1(S(t), I(t))$ and $Q_2(S(t), I(t))$ as

$$Q_1(S(t), I(t)) = \Lambda - \frac{\beta S I}{1 + \alpha S} - \delta S, \quad Q_2(S(t), I(t)) = \frac{\beta S I}{1 + \alpha S} - \gamma I - \delta I,$$

so we consider the following scalar differential equation:

$$\begin{cases} \dfrac{dI}{dS} = \dfrac{Q_2(S(t), I(t))}{Q_1(S(t), I(t))} = G(S, I), \\ I(ET) = I_0^+. \end{cases} \tag{2}$$

$G(S, I)$ is a continuously differentiable function. Now we denote $S_0^+ = S_c$, $I_0^+ = Y$ with $(S_0^+, I_0^+) \in N$. Then, we have

$$I(S) = I(S; S_c, Y) = I(S, Y)$$

and

$$I(S, Y) = Y + \int_{S_c}^{S} G(x, I(x, Y))dx,$$

where the value of S is between the L_M and the L_N.

Therefore, the Poincaré map P_M has the following form

$$P_M(Y) = (1 - \eta_2)I(S, Y).$$

Theorem 1. *For model (1) with $R_0 \leq 1$, the Poincaré map P_M exhibits the subsequent characteristics:*

(i) P_M has a domain spanning $[0, +\infty)$ and encompasses a range of $[0, P_M(I_T)]$.

(ii) Within the interval $[0, I_T]$, P_M exhibits an upward trend, but shows a decline for $(I_T, +\infty)$. It remains continuous and exhibits a concave nature over $[0, I_T]$.

(iii) The singular stable fixed point for P_M is at $I = 0$. Hence, model (1) possesses a stable disease-free periodic solution (DFPS).

Proof. It follows from the first function of system (2) that we have

$$\frac{\partial G(S,I)}{\partial I} = \frac{AB(C-qB)}{D^2}, \quad \frac{\partial^2 G(S,I)}{\partial I^2} = \frac{2CAB(C-qB)}{D^3},$$

where $A = \Lambda - \delta S$, $B = 1 + \alpha S$, $C = \beta S$, and

$$D = (\Lambda - \delta S)(1 + \alpha S) - \beta S I = AB - CS.$$

Given that $S < K$ and $R_0 \leq 1$, it follows that $A > 0$ and $C - qB < 0$, and for $I < I_T$, $D > 0$, whereas for $I > I_T$, $D < 0$. From these observations, it is clear that both

$$\frac{\partial G(S,I)}{\partial I} < 0 \text{ and } \frac{\partial^2 G(S,I)}{\partial I^2} < 0$$

hold true for every $I < I_T$.

From the principles of the Cauchy-Lipschitz theorem applied to the scalar differential equation, we can deduce that

$$\frac{\partial I(S,Y)}{\partial Y} = \exp\Big(\int_{S_c}^{S} \frac{\partial G(x, I(x,Y))}{\partial I} dx\Big) > 0$$

and

$$\frac{\partial^2 I(S,Y)}{\partial Y^2} = \exp\Big(\int_{S_c}^{S} \frac{\partial G(x, I(x,Y))}{\partial I} dx\Big) \int_{S_c}^{S} \frac{\partial^2 G(x, I(x,Y))}{\partial I^2} \frac{\partial I(x,Y)}{\partial Y} dx < 0.$$

Moreover, according to

$$P_M(Y) = (1 - \eta_2) I(S,Y),$$

we have

$$\frac{\partial P_M(Y)}{\partial Y} = (1-\eta_2)\frac{\partial I(S,Y)}{\partial Y} = (1-\eta_2)\exp\Big(\int_{S_c}^{S} \frac{\partial G(x, I(x,Y))}{\partial I} dx\Big)$$

and

$$\begin{aligned}\frac{\partial^2 P_M(Y)}{\partial Y^2} &= (1-\eta_2)\frac{\partial^2 I(S_t,Y)}{\partial Y^2} \\ &= (1-\eta_2)\exp\Big(\int_{S_c}^{S} \frac{\partial G(x, I(x,Y))}{\partial I} dx\Big) \int_{S_c}^{S} \frac{\partial^2 G(x, I(x,Y))}{\partial I^2} \frac{\partial I(x,Y)}{\partial Y} dx.\end{aligned}$$

Given that $(1 - \eta_2) > 0$, for $Y \in (0, I(T)]$, it is evident that

$$\frac{\partial P_M(Y)}{\partial Y} > 0 \text{ and } \frac{\partial^2 P_M(Y)}{\partial Y^2} < 0.$$

This suggests that $P_M(Y)$ is both continuously differentiable and concave within the interval $(0, I_T]$. Additionally, $P_M(Y)$ consistently rises within $(0, I_T]$ and falls in the range $(I_T, +\infty)$.

Therefore, when $R_0 \leq 1$, and taking into account that $\frac{ET}{u_1} < K$, it follows that for every Y in the sets $(0, I_T]$ and (I_T, K), the inequality $Y \geq I(S,Y) > P_M(Y)$ holds true. This implies that the Poincaré map P_M exhibits a singular fixed point which is globally stable. As a result, model (1) maintains a distinct DFPS that demonstrates global stability. □

4. The existence and stability of boundary order-1 periodic solution

If we define the function

$$f(S) = u_1 S + v_1(\Lambda - \delta S) - ET,$$

solving $L_M = 0$ yields the intersection points of L_M with the x-axis, which is equivalent to solving $f(S) = 0$. When $I = 0$, the model can be simplified as follows:

$$\begin{cases} \dfrac{dS(t)}{dt} = \Lambda - \delta S, & f(S) < 0, \\ S(t^+) = (1 - \eta_1)S(t), & f(S) = 0. \end{cases} \tag{3}$$

Furthermore, it follows from $f(S) = 0$ that we have

$$S_Z = \frac{ET - v_1\Lambda}{u_1 - v_1\delta},$$

so model (3) is equivalent to

$$\begin{cases} \dfrac{dS(t)}{dt} = \Lambda - \delta S, & S < S_Z, \\ S(t^+) = (1 - \eta_1)S(t), & S = S_Z. \end{cases} \tag{4}$$

Denoting the initial value $S_Z^+ = (1 - \eta_1)S_Z$, we have the following results:

Theorem 2. *If $R_0 \leq 1$, then system (1) has a globally stable boundary order-1 limit cycle $(S^T(t), 0)$ with period T, where*

$$S^T(t) = K + (S_Z^+ - K)\exp(-\delta t)$$

and

$$T = -\frac{1}{\delta}\ln(\frac{K - S_Z}{K - S_Z^+}).$$

Proof. Based on the premise that the solution $S(t)$ of the system moves from the initial value S_0 to S_Z within a finite time T, by solving the system with initial value $S_0 = S_Z^+$, we can conclude that the periodic solution

$$S^T(t) = K + (S_Z^+ - K)\exp(-\delta t)$$

and

$$\int_{S_Z^+}^{S_Z} \frac{1}{\Lambda - \delta S} dS = T.$$

Furthermore, it follows from in [38, Lemma A.1] that we have

$$\mu_2 = \Delta_K \exp \int_0^T \Big(\frac{\partial P(S^T(t), 0)}{\partial S} dt + \frac{\partial Q(S^T(t), 0)}{\partial I} dt\Big),$$

where

$$\Delta_K = \frac{P^+\Big(\dfrac{\partial \beta}{\partial I}\dfrac{\partial \phi}{\partial S} - \dfrac{\partial \beta}{\partial S}\dfrac{\partial \phi}{\partial I} + \dfrac{\partial \phi}{\partial S}\Big) + Q^+\Big(\dfrac{\partial \alpha}{\partial S}\dfrac{\partial \phi}{\partial I} - \dfrac{\partial \alpha}{\partial I}\dfrac{\partial \phi}{\partial S} + \dfrac{\partial \phi}{\partial I}\Big)}{P\dfrac{\partial \phi}{\partial S} + Q\dfrac{\partial \phi}{\partial I}},$$

$$P(S,I) = \Lambda - \frac{\beta S I}{1+\alpha S} - \delta S, \quad Q(S,I) = \frac{\beta S I}{1+\alpha S} - \gamma I - \delta I,$$
$$\alpha(S,I) = -\eta_1 S, \quad \beta(S,I) = -\eta_2 I\phi(S,I) = u_1 S + v_1 P(S,I) - ET.$$

By simple calculations, we have

$$\frac{\partial\phi(S^T(t),0)}{\partial S} = u_1 - v_1\delta, \quad \frac{\partial\beta(S^T(t),0)}{\partial I} = -\eta_2$$

and

$$Q(S^T(t),0) = Q(S^{T^+}(t),0) = 0,$$

which yields

$$\Delta_K = \frac{(1-\eta_2)(K - S_Z^+)}{K - S_Z}.$$

Moreover, we can obtain

$$\exp\int_0^T \Big(\frac{\partial P(S^T(t),0)}{\partial S}dt + \frac{\partial Q(S^T(t),0)}{\partial I}dt\Big) = \exp\int_0^T \Big(\frac{\beta S^T(t)}{1+\alpha S^T(t)} - \delta - q\Big)dt,$$

where

$$\begin{aligned}\int_0^T \frac{\beta S^T(t)}{1+\alpha S^T(t)}dt &= \int_{S_Z^+}^{S_Z} \frac{\beta S}{(1+\alpha S)(\Lambda - \delta S)}dS \\ &= -\frac{\beta}{\Lambda\alpha+\delta}\Big(\frac{1}{\delta}\ln\frac{1+\alpha S_Z}{1+\alpha S_Z^+} + K\ln\frac{K-S_Z}{K-S_Z^+}\Big),\end{aligned}$$

$$\int_0^T (-\delta) = \ln\frac{K-S_Z}{K-S_Z^+}$$

and

$$\int_0^T (-q) = \frac{q}{\delta}\ln\frac{K-S_Z}{K-S_Z^+}.$$

Therefore,

$$\mu_2 = (1-\eta_2)\exp\Big(-\frac{1}{\Lambda\alpha+\delta}\Big[\frac{\beta}{\alpha}\ln\frac{1+\alpha S_Z}{1+\alpha S_Z^+} + q(R_0-1)\ln\frac{K-S_Z}{K-S_Z^+}\Big]\Big),$$

so we can know that $\mu_2 < 1$ for $R_0 < 1$, which means that the boundary order-1 limit cycle $(S^T(t),0)$ is orbitally asymptotically stable.

Once it is established that the boundary order-1 limit cycle $(S^T(t),0)$ is globally attractive, it is tantamount to demonstrating its global stability. Thus, we make the assumption that the pulse point sequence I_k^+ for $k \geq 0$ lies entirely on the line L_N and $I_k^+ \in [0,(1-\eta_2)I_{T1}]$. Given that $R_0 \leq 1$, we can deduce that $\dfrac{dI}{dt} < 0$ for $S < K$. Consequently, we can ascertain that I_k^+ forms a strictly decreasing sequence, with

$$\lim_{k\to+\infty} I_k^+ = I_0.$$

Additionally, the monotonicity of $I(t)$, as depicted in Figure 2a, dictates that $I_0 = 0$. As a result, the boundary order-1 limit cycle $(S^T(t),0)$ for model (1) is globally attractive. This completes the proof of Theorem 2. □

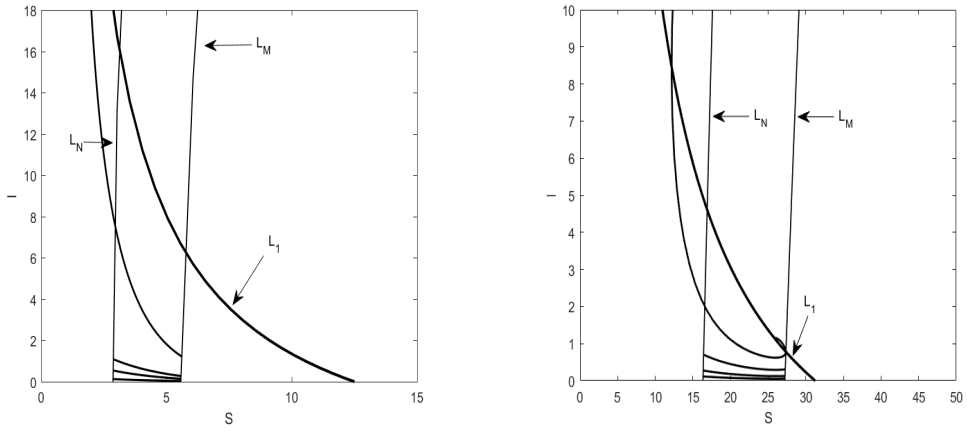

Figure 2. Illustration of the global stability of the DFPS with $ET = 3$ in (a) and bistability with $ET = 19.15$ in (b). The fixed parameter values are $\Lambda = 2.5$, $\beta = 0.015$, $\alpha = 0.001$, $\delta = 0.08$, $\gamma = 0.3$, $\eta_1 = 0.4$, $\eta_2 = 0.1$, $u_1 = 0.7$, $v_1 = 0.3$.

5. Bifurcations for $R_0 > 1$

5.1. Transcritical bifurcations for ET

According to

$$S_Z = \frac{ET - v_1\Lambda}{u_1 - v_1\delta},$$

taking the derivative of μ_2 with respect to ET as

$$\frac{d\mu_2}{dET} = \frac{d\mu_2}{dS_Z}\frac{dS_Z}{dET} = \frac{\mu_2}{u_1 - v_1\delta}(g(S_Z) - (1-\eta_1)g(S_Z^+)),$$

where

$$g(S) = \frac{(\beta - \alpha q)S - q}{(1+\alpha S)(\Lambda - \delta S)},$$

taking the derivative of $g(S)$ with respect to S yields

$$\begin{aligned} g'(S) &= \frac{(\beta-\alpha q)((1+\alpha S)(\Lambda-\delta S) - (S-S^*)(\alpha\Lambda - \delta - 2\alpha\delta S))}{((1+\alpha S)(\Lambda-\delta S))^2} \\ &= \frac{(\beta-\alpha q)g_2(S)}{((1+\alpha S)(\Lambda-\delta S))^2}, \end{aligned}$$

where

$$g_2(S) = (\alpha\delta S^2 - 2\alpha\delta S^* S + (\alpha\Lambda - \delta)S^* + \Lambda).$$

By simple calculations, we know that $g_2(S)$ has a minimum value $(-\alpha\delta(S^*)^2 + (\alpha\Lambda - \delta)S^* + \Lambda)$ for $S = S^*$, and if

$$-\frac{1}{\alpha} < S^* < K, \quad (i.e.,\ R_0 > 1),$$

then

$$(-\alpha\delta(S^*)^2 + (\alpha\Lambda - \delta)S^* + \Lambda) > 0,$$

and then $g^{'}(S) > 0$.

Based on the above discussion, if

$$S_Z > S^* \geq S_Z^+,$$

then

$$g(S_Z) > 0 \geq g(S_Z^+)$$

and

$$g(S_Z) - (1 - \eta_1)g(S_Z^+) > 0.$$

If

$$S_Z > S_Z^+ > S^*,$$

then

$$g(S_Z) > g(S_Z^+) > 0$$

and

$$g(S_Z) - (1 - \eta_1)g(S_Z^+) > 0.$$

Moreover, it is clear that

$$\int_{S_Z^+}^{S_Z} g(S)dS < 0$$

as S_Z approaches S^*, and

$$\int_{S_Z^+}^{S_Z} g(S)dS = +\infty$$

as S_Z approaches K. According to the monotonicity of $\int_{S_Z^+}^{S_Z} g(S)dS$, it can be inferred that there is an

$$ET^* \in ((u_1 - v_1\delta)S^* + v_1\Lambda, (u_1 - v_1\delta)K + v_1\Lambda),$$

such that $\mu_2 = 1$.

It is clear that

$$P_M(0, ET) = I(S_Z, 0) = 0,$$

and it follows from the definition of P_M that we have

$$\frac{\partial P_M(0, ET^*)}{\partial Y} = \mu_2(ET^*) = (1 - \eta_2)\exp\Big(\int_{S_Z^+}^{S_Z} \frac{\partial G(x, I(x, Y))}{\partial I}dx\Big) = 1.$$

According to the monotonicity of $g(S)$, it can be known that

$$\frac{\partial^2 P_M(0, ET^*)}{\partial Y \partial ET} = \frac{d\mu_2(ET^*)}{dET} > 0,$$

$$\frac{\partial^2 P_M(0, ET^*)}{\partial Y^2} = (1 - \eta_2)\exp\Big(\int_{S_c}^{S} \frac{\partial G(x, I(x, Y))}{\partial I}dx\Big)\int_{S_c}^{S} \frac{\partial^2 G(x, I(x, Y))}{\partial I^2}\frac{\partial I(x, Y)}{\partial Y}dx.$$

To simplify symbols, now we denote

$$\begin{aligned}
E_1(x) &= \int_{S_Z^+}^{x} \frac{(\beta-\alpha q)x-q}{(\Lambda-\delta x)(1+\alpha x)}dx,\\
E_2(x) &= (1-\eta_2)\exp(E_1(x)),\\
E_3(x) &= \frac{\partial^2}{\partial I^2}G(x,I(x,0)) = \frac{2\beta x((\beta-\alpha q)x-q)}{((\Lambda-\delta x)(1+\alpha x))^2},\\
E_4(x) &= \frac{E_3(x)}{E_1^{'}(x)} = \frac{2\beta x}{(\Lambda-\delta x)(1+\alpha x)}.
\end{aligned}$$

By simple calculations, we have

$$E_2(S_Z^+) = 1-\eta_2 \ \text{ and } \ E_2(S_Z) = \mu_2(ET).$$

For convenience, we derive the derivative of $E_1(x)$ with respect to x as

$$E_1^{'}(x) = \frac{(\beta-\alpha q)x-q}{(\Lambda-\delta x)(1+\alpha x)}.$$

Therefore, through inequality A, we can obtain

$$\begin{aligned}
\frac{\partial^2 P_M(0,ET^*)}{\partial Y^2} &= \int_{S_Z^+}^{S_Z} \frac{\partial^2}{\partial I^2}(G(x,I(x,0)))\frac{\partial I(x,0)}{\partial Y}dx\\
&= \frac{1}{1-\eta_2}\int_{S_Z^+}^{S_Z} E_3(x)E_2(x)dx\\
&= \frac{1}{1-\eta_2}\int_{S_Z^+}^{S_Z} \frac{E_3(x)}{E_1^{'}(x)}d(E_2(x))\\
&= \frac{1}{1-\eta_2}\int_{S_Z^+}^{S_Z} E_4(x)d(E_2(x)).
\end{aligned}$$

According to the monotonicity of $E_1(x)$, we know that the function $E_2(x)$ is monotonically decreasing for $x \in [S_Z^+, S^*]$ and monotonically increasing for $x \in [S^*, S_Z]$. Thus, if $ET = ET^*$, then

$$E_2(S_Z^+) = 1-\eta_2 \ \text{ and } \ E_2(S_Z) = \mu_2(ET^*) = 1,$$

which indicates that $E_2(S^*) < E_2(x) \le 1$ for all $x \in [S_Z^+, S_Z]$. Moreover, we have

$$E_4^{'}(x) = \frac{2\beta(\Lambda+\delta\alpha x^2)}{((\Lambda-\delta x)(1+\alpha x))^2} > 0,$$

and thus, $E_4(x) > 0$ is monotonically increasing on $[S_Z^+, S_Z]$. Furthermore, we have

$$\begin{aligned}
\int_{S_Z^+}^{S_Z} E_4(x)d(E_2(x)) &= E_2(x)E_4(x)|_{S_Z^+}^{S_Z} - \int_{S_Z^+}^{S_Z} E_2(x)E_4^{'}(x)dx\\
&= E_4(S_Z) - (1-\eta_2)E_4(S_Z^+) - \int_{S_Z^+}^{S_Z} E_2(x)E_4^{'}(x)dx\\
&> E_4(S_Z) - E_4(S_Z^+) - \int_{S_Z^+}^{S_Z} E_2(x)E_4^{'}(x)dx.
\end{aligned}$$

By simple calculations, we have

$$E_4(S_Z) - E_4(S_Z^+) - \int_{S_Z^+}^{S_Z} E_2(x)E_4^{'}(x)dx = \int_{S_Z^+}^{S_Z} (1 - E_2(x))E_4^{'}(x)dx,$$

which means that

$$\frac{\partial^2 P_M(0, ET^*)}{\partial Y^2} > 0.$$

The above calculations demonstrate that the conditions of in [38, Lemma A.2] are satisfied. Therefore, we have the following conclusion:

Theorem 3. *Given that $S^* < S_Z < K$ and $R_0 > 1$, $P_M(Y, ET)$ undergoes a transcritical bifurcation at $ET = ET^*$. This indicates the emergence of an unstable positive fixed point for $P_M(Y, ET)$ as ET transitions across ET^* from the right to the left side. Consequently, we posit that for some sufficiently small value $\epsilon > 0$, system (1) exhibits an unstable positive periodic solution when ET lies in the interval $(ET^* - \epsilon, ET^*)$.*

The emergence of a positive fixed point as elucidated in Theorem 3 indicates an unstable positive periodic solution for system (1). This suggests a concurrent local stability of the internal equilibrium (S^*, I^*) and the DFPS in system (1), leading to what we refer to as a bistable impulsive system, as shown Figure 2b. A more precise description is provided below.

Theorem 4. *Given conditions $S^* < S_Z < K$, $R_0 > 1$, and $ET \in (ET^* - \epsilon, ET^*)$, where $\epsilon > 0$ is sufficiently small, it can be concluded that system (1) exhibits bistability.*

5.2. Transcritical bifurcations for η_1

Here we take η_1 as the key factor for bifurcation. Thus, we have

$$\mu_2(\eta_1) = (1 - \eta_2) \exp\Big(\int_{S_Z^+}^{S_Z} \frac{(\beta - \alpha q)S - q}{(1 + \alpha S)(\Lambda - \delta S)} dS \Big).$$

By simple calculation, we have

$$\frac{d\mu_2(\eta_1)}{d\eta_1} = S_Z(1 - \eta_2) \frac{(\beta - \alpha q)S_Z^+ - q}{(1 + \alpha S_Z^+)(\Lambda - \delta S_Z^+)} \exp\Big(\int_{S_Z^+}^{S_Z} \frac{(\beta - \alpha q)S - q}{(1 + \alpha S)(\Lambda - \delta S)} dS \Big),$$

and solving

$$\frac{d\mu_2(\eta_1)}{d\eta_1} = 0$$

yields a unique root $S_Z^+ = S^*$, i.e.,

$$\frac{d\mu_2(\overline{\eta}_1)}{d\eta_1} = 0,$$

where

$$\overline{\eta}_1 = 1 - \frac{S^*}{S_Z}.$$

From the given information, for η_1 in the range $(0, \overline{\eta}_1)$, it is evident that

$$S_Z^+ > S^* \text{ and } \frac{d\mu_2(\eta_1)}{d\eta_1} > 0.$$

Conversely, for η_1 in the interval $(\overline{\eta}_1, 1)$, we observe that

$$S_Z^+ < S^* \text{ and } \frac{d\mu_2(\eta_1)}{d\eta_1} < 0.$$

According to the monotonicity of $\frac{d\mu_2(\eta_1)}{d\eta_1}$, it is clear that the value of $\mu_2(0)$ is less than that of $\mu_2(\overline{\eta}_1)$, denoting that $\mu_2(\eta_1)$ shows an increasing trend in the interval $[0, \overline{\eta}_1]$ and a decreasing trend when η_1 lies between $(\overline{\eta}_1, 1)$. Moreover, guided by the trend in the rate of change, if $\mu_2(\overline{\eta}_1) > 1$, a particular value η_1^* exists in the interval $(0, \overline{\eta}_1)$ for which $\mu_2(\eta_1^*) = 1$. Similarly, if $\mu_2(1) < 1$, there exists a singular value η_1^{**} in the range $(\overline{\eta}_1, 1)$ such that $\mu_2(\eta_1^{**}) = 1$. If $\eta_1 = \overline{\eta}_1$, it follows from

$$\ln \frac{K - S_Z^+}{K - S_Z} > 1 - \frac{K - S_Z}{K - S_Z^+} = \frac{S_Z - S_Z^+}{K - S_Z^+}$$

and

$$\ln \frac{1 + \alpha S_Z}{1 + \alpha S_Z^+} < \frac{1 + \alpha S_Z}{1 + \alpha S_Z^+},$$

that we have

$$\begin{aligned}
&\frac{1}{\Lambda\alpha + \delta}\left(q(R_0 - 1) \ln \frac{K - S_Z^+}{K - S_Z} - \frac{\beta}{\alpha} \ln \frac{1 + \alpha S_Z}{1 + \alpha S_Z^+}\right) \\
&> \frac{1}{\Lambda\alpha + \delta}\left(q(R_0 - 1) \frac{S_Z - S_Z^+}{K - S_Z^+} - \frac{\beta(1 + \alpha S_Z)}{\alpha(1 + \alpha S_Z^+)}\right) \\
&> \frac{1}{\Lambda\alpha + \delta}\left(q(R_0 - 1) \frac{\overline{\eta}_1 S_Z}{K - S_Z} - \frac{\beta(1 + \alpha S_Z)}{\alpha}\right).
\end{aligned}$$

If

$$\frac{1}{\Lambda\alpha + \delta}\left(q(R_0 - 1) \frac{\overline{\eta}_1 S_Z}{K - S_Z} - \frac{\beta(1 + \alpha S_Z)}{\alpha}\right) > \ln \frac{1}{1 - \eta_2},$$

then

$$1 > \overline{\eta}_1 > \left((\Lambda\alpha + \delta) \ln \frac{1}{1 - \eta_2} + \frac{\beta(1 + \alpha S_Z)}{\alpha}\right) \frac{(K - S_Z)}{q(R_0 - 1) S_Z},$$

and then $\mu_2(\overline{\eta}_1) > 1$.

If $\eta_1 = 1$, then $S_Z^+ = 0$. It follows from

$$\ln \frac{K - S_Z^+}{K - S_Z} < \frac{K - S_Z^+}{K - S_Z}$$

and

$$\ln \frac{1 + \alpha S_Z}{1 + \alpha S_Z^+} > \frac{\alpha(S_Z - S_Z^+)}{1 + \alpha S_Z},$$

that we have

$$\frac{1}{\Lambda\alpha+\delta}\Big(q(R_0-1)\ln\frac{K-S_Z^+}{K-S_Z}-\frac{\beta}{\alpha}\ln\frac{1+\alpha S_Z}{1+\alpha S_Z^+}\Big)<\frac{1}{\Lambda\alpha+\delta}\Big(q(R_0-1)\frac{K}{K-S_Z}-\frac{\beta S_Z}{(1+\alpha S_Z)}\Big).$$

If

$$\frac{1}{\Lambda\alpha+\delta}\Big(q(R_0-1)\frac{K}{K-S_Z}-\frac{\beta S_Z}{(1+\alpha S_Z)}\Big)<\ln\frac{1}{1-\eta_2},$$

then

$$1<R_0<1+\frac{(K-S_Z)}{Kq}\Big((\Lambda\alpha+\delta)\ln\frac{1}{1-\eta_2}+\frac{\beta S_Z}{(1+\alpha S_Z)}\Big),$$

and then $\mu_2(1)<1$.

Therefore, from the above discussion, we can derive the following results according to in [38, Lemma A.2].

Theorem 5. *Given the conditions $S^*<S_Z<K$ and $\mu_2(\overline{\eta}_1)>1>\mu_2(1)$, there exist transcritical bifurcation points denoted by $\eta_1=\eta_1^*$ and $\eta_1=\eta_1^{**}$ for $P_M(Y,\eta_1)$. This indicates that, as the parameter η_1 surpasses η_1^* in the decreasing direction, or goes beyond η_1^{**} in the increasing direction, $P_M(Y,\eta_1)$ establishes an unstable positive equilibrium point. Under the presumption of a sufficiently diminutive value $\epsilon>0$, system (1) demonstrates an unstable positive periodic solution when η_1 is situated in either the interval $(\eta_1^*-\epsilon,\eta_1^*)$ or $(\eta_1^{**},\eta_1^{**}+\epsilon)$.*

Proof. It is obvious that

$$P_M(0,\eta_1)=I(S_Z,0)=0.$$

It follows from the proof of Theorem 1 that we have

$$\frac{\partial P_M(0,\eta_1)}{\partial Y}=(1-\eta_2)\exp\Big(\int_{S_Z^+}^{S_Z}\frac{(\beta-\alpha q)S-q}{(1+\alpha S)(\Lambda-\delta S)}dS\Big)=\mu_2(\eta_1).$$

Thus,

$$\frac{\partial P_M(0,\eta_1^*)}{\partial Y}=\mu_2(\eta_1^*)=1,$$

and we have

$$\frac{\partial^2 P_M(0,\eta_1)}{\partial Y\partial\eta_1}=\frac{d\mu_2(\eta_1)}{d\eta_1},$$

which means that

$$\frac{\partial^2 P_M(0,\eta_1^*)}{\partial Y\partial\eta_1}=\frac{d\mu_2(\eta_1^*)}{d\eta_1}>0$$

and

$$\frac{\partial^2 P_M(0,\eta_1^{**})}{\partial Y\partial\eta_1}=\frac{d\mu_2(\eta_1^{**})}{d\eta_1}<0.$$

Through the similarity method in the proof process of Theorem 3, we have

$$\frac{\partial^2 P_M(0,\eta_1^*)}{\partial Y^2}>0\ \text{ and }\ \frac{\partial^2 P_M(0,\eta_1^{**})}{\partial Y^2}>0.$$

Consequently, under the conditions $S^*<S_Z<K$, $\mu_2(\overline{\eta}_1)>1$, and $1>\mu_2(1)$, $P_M(Y,\eta_1)$ results in an unstable fixed point when η_1 transitions past η_1^* in a right-to-left direction or η_1^{**} in a left-to-right direction. Moreover, given $\eta_1\in(\eta_1^*-\epsilon,\eta_1^*)$ or $\eta_1\in(\eta_1^{**},\eta_1^{**}+\epsilon)$, where $\epsilon>0$ is sufficiently small, system (1) has an unstable positive periodic solution. This concludes our demonstration. □

6. Numerical simulation and analysis

We observe the extent to which the model is affected by varying the weighted coefficients, u_1 and v_1, of the action threshold. When we set u_1 and v_1, as shown in Figure 3a, L_M and L_N become two lines perpendicular to the x-axis. At this point, the model is simplified to a pulse system with the threshold based solely on the density of susceptible individuals. Such systems have been extensively studied and widely applied in infectious diseases and population dynamics.

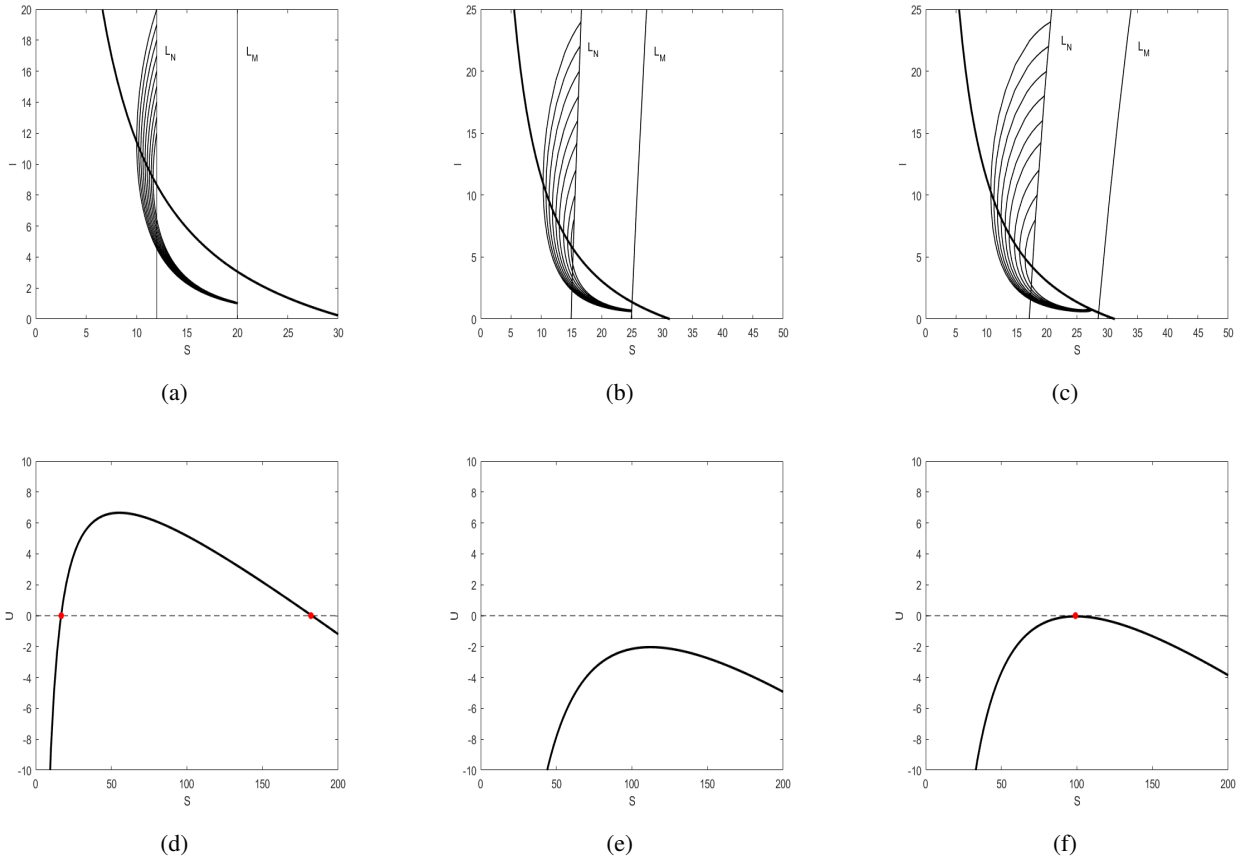

Figure 3. The trajectories of system (1) under various action thresholds. $ET = 20$ in (a)–(c); $u_1 = 0.7$, $v_1 = 0.3$ in (d)–(f). The fixed parameter values are $\Lambda = 2.5$, $\beta = 0.015$, $\alpha = 0.001$, $\delta = 0.08$, $\gamma = 0.3$, $\eta_1 = 0.4$, $\eta_2 = 0.1$.

However, when the rate of change is introduced into the action threshold, L_M and L_N become two curves, and the curvature of these curves varies with changes in u_1 and v_1, Figure 3b,c highlights the influence of the rate of change of susceptible individuals in the implementation of a comprehensive control strategy. Properly choosing the coefficients can lead to the virus becoming extinct after a finite number of control measures.

When v_1 is non-zero, L_M and L_N represent two curves, and there is a possibility of intersection between them. We define $U = L_M - L_N$. By varying the value of ET, we can observe whether there are intersections between the pulse set and phase set. Figure 3d–f shows that as ET increases, the number

of intersections decreases from 2 to 0. The presence of intersections poses challenges in the analysis of Poincaré maps, leading to highly complex dynamics. This complexity is a primary focus of our ongoing research.

In previous sections, we explored the possibility of bifurcations with respect to individual parameters, as depicted in Figure 4. To examine the sensitivity of the model, we further investigated the impact of different weighted coefficients for the action threshold as influencing factors on bifurcations.

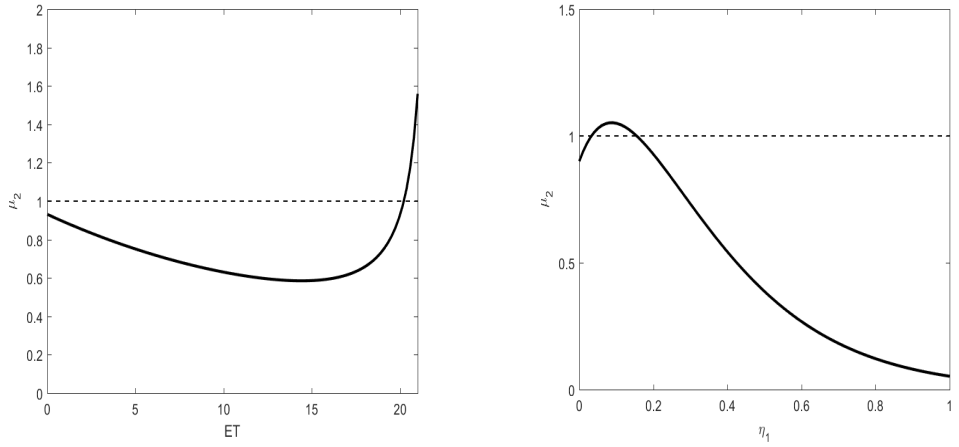

(a) (b)

Figure 4. The graph illustrates the Floquet multiplier μ_2 as a function of the parameters ET and η_1. Parameter $\eta_1 = 0.2$ in (a); $ET = 20$ in (b); and other fixed parameter values are $\Lambda = 2.5, \beta = 0.015, \alpha = 0.001, \delta = 0.08, \gamma = 0.3, \eta_2 = 0.1, u_1 = 0.7, v_1 = 0.3$.

In Figure 5a,b, as the parameter v_1 increases, the trajectories of μ_2 concerning ET intersect with the line $\mu_2 = 1$ at two distinct points. Specifically, with v_1 rising from 0.5 to 0.65, two intersections with the line $\mu_2 = 1$ are highlighted. However, Figure 5c,d depict that, as v_1 decreases, the peak values of μ_2's trajectories in relation to η_1 diminish, eventually dropping below 1. Collectively, these patterns suggest that considering the rate of change in the action threshold is a more comprehensive approach for managing infectious diseases, emphasizing the importance of monitoring not just the current thresholds, but their evolution over time.

In Figure 6a–c, the float multiplier μ_2 response to the action threshold ET is closely related to multiple parameters. First, with an increase in the birth rate, Λ, the initial value of μ_2 in the low ET region rises, suggesting that a higher threshold might be needed to maintain stability of μ_2 at a higher birth rate. Further considering the maximum vaccination rate η_1, its increase results in a slight rise in the initial point of μ_2 at low ET, indicating an enhanced sensitivity of μ_2 to the threshold under high vaccination scenarios. Additionally, for the maximum treatment rate η_2, similar μ_2 trajectories are given at low ET values, but with a higher value of η_2, the decline trend of μ_2 is more rapid. This reveals that, in a high treatment rate environment, μ_2 responds more quickly to threshold changes. In summary, these analyses present how the relationship between μ_2 and ET is influenced by the three parameters Λ, η_1, and η_2.

On the other hand, in Figure 6d–f, the relationship between μ_2 and the maximum vaccination rate

η_1 is significantly affected by different parameters. For instance, when the birth rate Λ rises from 2.3 to 2.7, the peak value of μ_2 consistently increases and shifts to the right. For scenarios where η_1 is close to 1, all μ_2 trajectories are approximately 0. When the focus is on the maximum treatment rate η_2, even though peak positions of the trajectories are similar, with the growth of η_2, the peak gradually decreases; especially in parts where η_1 is larger, the decline of μ_2 is more pronounced. For the threshold ET, as it increases from 18 to 21, the maximum value of μ_2 seems to decrease, and its peak position shifts to the right. This aligns with the observation of μ_2 trajectories approaching 0 when η_1 is near 1. These shifts provide a comprehensive view of how the system adjusts based on different parameter values.

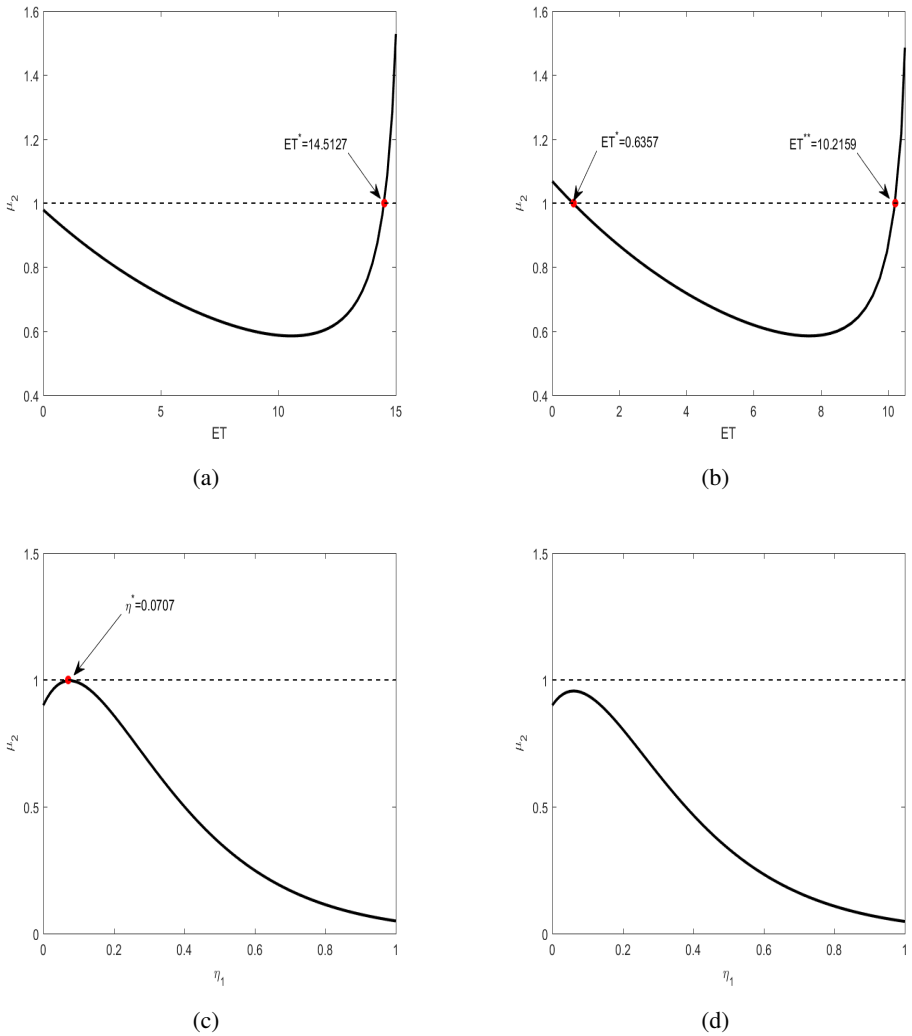

Figure 5. The figure illustrates how the Floquet multiplier μ_2 varies as a function of the parameters ET and η_1, under the influence of changing values of u_1 and v_1. Parameter $\eta_1 = 0.2$ in (a), (b); $ET = 20$ in (c), (d). The fixed parameter values are $\Lambda = 2.5$, $\beta = 0.015$, $\alpha = 0.001$, $\delta = 0.08$, $\gamma = 0.3$, $\eta_2 = 0.1$.

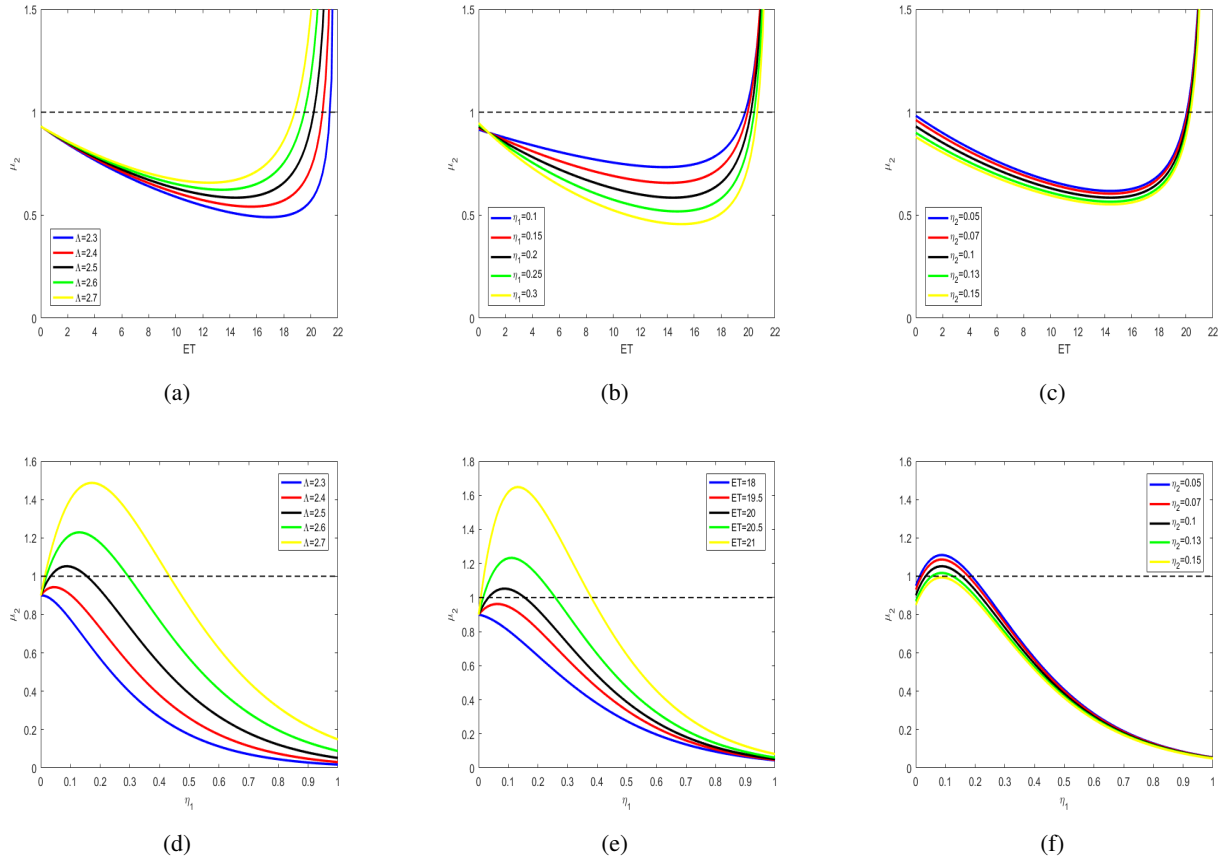

Figure 6. Comprehensive analysis of the response of μ_2 to ET and η_1 and its relationship with various parameters. $\eta_1 = 0.2$ in (a), (c); $\eta_2 = 0.1$ in (a), (b), (d) and (e); $\Lambda = 2.5$ in (b), (c), (e) and (f); $ET = 20$ in (d), (f). The fixed parameter values are $\beta = 0.015$, $\alpha = 0.001$, $\delta = 0.08$, $\gamma = 0.3$, $u_1 = 0.7$, $v_1 = 0.3$.

7. Conclusions and discussion

In conclusion, state-dependent impulsive semi-dynamic systems represent a category of highly discontinuous and non-smooth systems. These systems have been applied in various fields, including integrated pest management, viral dynamical systems, and diabetes treatment [26, 39–41]. In recent years, significant progress has been made in the research of such systems, encompassing analytical techniques, qualitative analyses, and practical applications [30, 42]. Notably, the Poincaré map serves as a mathematical tool promoting comprehensive exploration of impulsive systems with nonlinear impulsive functions, enabling the study of the existence and global stability of k-order periodic solutions.

In our research, we examined a state-dependent impulsive model, which incorporates a saturation incidence rate and describes the interaction between susceptibles and infectives. A highlight is that the action threshold in our model is determined by the density of susceptibles and its rate of change. This differentiates our work from previous literature [37,38], which primarily operated under the assumption of a fixed action threshold. Our innovation lies in introducing an action threshold determined by the

density of the affected susceptibles and its rate of change, thereby translating the impulse set and phase set into more intricate nonlinear curves.

By analyzing the various positional relationships between system trajectories and equilibrium points, we derived the respective impulse and phase sets, as depicted in Figure 1. Utilizing these conditions, we constructed the Poincaré map and studied the conditions for the emergence of a first-order periodic solution within the system framework. Furthermore, we undertook a thorough examination of the stability of these first-order periodic solutions. Our theoretical findings were corroborated by numerical simulations, confirming the existence of the first-order periodic solution. Additionally, based on the results of the single parameter's influence on μ_2, we conducted a sensitivity analysis by fixing other parameters and selecting one parameter as a benchmark to observe the trajectory changes of μ_2, as shown in Figure 4. Under certain conditions, the threshold parameter ET or vaccination rate η_1 can induce a transcritical bifurcation, leading to unstable positive periodic solutions. Boundary periodic solutions and equilibrium points of the impulse-free system can coexist, suggesting the possibility of backward bifurcations. Importantly, when the action threshold ET is weighted by the density of susceptible individuals and its rate of change, the impulse curve and phase curve become nonlinear, as shown in Figure 3. The system's impulse curve, phase curve, and the intricate and mutable positional relationships between them and two isoclines introduce complexity, making the precise definition of the boundaries of impulse and phase sets challenging. Furthermore, based on Figure 5, variations in the weighted values of the susceptible individual density and its rate of change also impact the bifurcation results of the model. According to Figure 6, μ_2 responds to the action threshold ET based on several parameters, including birth rate, maximum vaccination rate, and maximum treatment rate. Among them, the relationship between μ_2 and vaccination rate η_1 is also significantly influenced by the birth rate, maximum treatment rate, and action threshold.

Finally, we emphasize the critical role of mathematical models and control strategies in the field of infectious disease control. Future research directions may delve deeper into considering the growth rate of infected individuals as a threshold for studying disease control strategies, thereby advancing the development of more complex nonlinear pulse control methods. The further application of this technology holds the potential to have a profound impact on infectious disease control and other related fields, providing valuable directions for future research and application.

Use of AI tools declaration

The authors declare they have not used Artificial Intelligence (AI) tools in the creation of this article.

Acknowledgments

This work is supported by the National Natural Science Foundation of China (No. 12261033).

Conflict of interest

The authors declare no conflicts of interest.

References

1. O. Diekmann, J. A. P. Heesterbeek, J. A. Metz, On the definition and the computation of the basic reproduction ratio R_0 in models for infectious diseases in heterogeneous populations, *J. Math. Biol.*, **28** (1990), 365–382. https://doi.org/10.1007/BF00178324
2. A. B. Sabin, Measles, killer of millions in developing countries: strategy for rapid elimination and continuing control, *Eur. J. Epidemiol.*, **7** (1991), 1–22. https://doi.org/10.1007/BF00221337
3. C. A. de Quadros, J. K. Andrus, J. M. Olivé, C. M. da Silveira, R. M. Eikhof, P. Carrasco, et al., Eradication of poliomyelitis: progress in the Americas, *Pediatr. Infect. Dis. J.*, **10** (1991), 222–229. https://doi.org/10.1097/00006454-199103000-00011
4. M. Ramsay, N. Gay, E. Miller, M. Rush, J. White, P. Morgan-Capner, et al., The epidemiology of measles in England and Wales: rationale for the 1994 national vaccination campaign, *Commun. Dis. Rep.*, **4** (1994), R141–R146.
5. A. Khan, J. F. Gómez-Aguilar, T. S. Khan, H. Khan, Stability analysis and numerical solutions of fractional order HIV/AIDS model, *Chaos Solitons Fract.*, **122** (2019), 119–128. https://doi.org/10.1016/j.chaos.2019.03.022
6. H. Khan, J. F. Gómez-Aguilar, A. Alkhazzan, A. Khan, A fractional order HIV-TB coinfection model with nonsingular Mittag-Leffler law, *Math. Methods Appl. Sci.*, **43** (2020), 6. https://doi.org/10.1002/mma.6155
7. A. Khan, H. M. Alshehri, T. Abdeljawad, Q. M. Al-Mdallal, H. Khan, Stability analysis of fractional nabla difference COVID-19 model, *Results Phys.*, **22** (2021), 103888. https://doi.org/10.1016/j.rinp.2021.103888
8. R. Begum, O. Tunç, H. Khan, H. Gulzar, A. Khan, A fractional order Zika virus model with Mittag-Leffler kernel, *Chaos Solitons Fract.*, **146** (2021), 110898. https://doi.org/10.1016/j.chaos.2021.110898
9. M. Aslam, R. Murtaza, T. Abdeljawad, G. U. Rahman, A. Khan, H. Khan, et al., A fractional order HIV/AIDS epidemic model with Mittag-Leffler kernel, *Adv. Differ. Equations*, **2021** (2021), 107. https://doi.org/10.1186/s13662-021-03264-5
10. Q. T. Ain, A. Khan, T. Abdeljawad, J. F. Gómez-Aguilar, S. Riaz, Dynamical study of varicella-zoster virus model in sense of Mittag-Leffler kernel, *Int. J. Biomath.*, **17** (2024), 2350027. https://doi.org/10.1142/S1793524523500274
11. G. R. Jiang, Q. G. Yang, Periodic solutions and bifurcation in an SIS epidemic model with birth pulses, *Math. Comput. Modell.*, **50** (2009), 498–508. https://doi.org/10.1016/j.mcm.2009.04.021
12. Q. Q. Zhang, S. Y. Tang, X. F. Zou, Rich dynamics of a predator-prey system with state-dependent impulsive controls switching between two means, *J. Differ. Equations*, **364** (2023), 336–377. https://doi.org/10.1016/j.jde.2023.03.030
13. S. J. Gao, L. S. Chen, Z. D. Teng, Impulsive vaccination of an SEIRS model with time delay and varying total population size, *Bull. Math. Biol.*, **69** (2007), 731–745. https://doi.org/10.1007/s11538-006-9149-x

14. J. C. Panetta, A mathematical model of periodically pulsed chemotherapy: tumor recurrence and metastasis in a competitive environment, *Bull. Math. Biol.*, **58** (1996), 425–447. https://doi.org/10.1007/BF02460591

15. S. Bunimovich-Mendrazitsky, H. Byrne, L. Stone, Mathematical model of pulsed immunotherapy for superficial bladder cancer, *Bull. Math. Biol.*, **70** (2008), 2055–2076. https://doi.org/10.1007/s11538-008-9344-z

16. Q. Li, Y. N. Xiao, Dynamical behavior and bifurcation analysis of the SIR model with continuous treatment and state-dependent impulsive control, *Int. J. Bifurcat. Chaos*, **29** (2019), 1950131. https://doi.org/10.1142/S0218127419501311

17. Z. L. He, J. G. Li, L. F. Nie, Z. Zhao, Nonlinear state-dependent feedback control strategy in the SIR epidemic model with resource limitation, *Adv. Differ. Equations*, **2017** (2017), 209. https://doi.org/10.1186/s13662-017-1229-8

18. S. Y. Tang, Y. N. Xiao, D. Clancy, New modelling approach concerning integrated disease control and cost-effectivity, *Nonlinear Anal.*, **63** (2005), 439–471. https://doi.org/10.1016/j.na.2005.05.029

19. L. F. Nie, Z. D. Teng, A. Torres, Dynamic analysis of an SIR epidemic model with state dependent pulse vaccination, *Nonlinear. Anal.*, **13** (2012), 1621–1629. https://doi.org/10.1016/j.nonrwa.2011.11.019

20. L. F. Nie, Z. D. Teng, B. Z. Guo, A state dependent pulse control strategy for a SIRS epidemic system, *Bull. Math. Biol.*, **75** (2013), 1697–1715. https://doi.org/10.1007/s11538-013-9865-y

21. X. W. Yu, S. L. Yuan, T. H. Zhang, Asymptotic properties of stochastic nutrient-plankton food chain models with nutrient recycling, *Nonlinear. Anal.*, **34** (2019), 209–225. https://doi.org/10.1016/j.nahs.2019.06.005

22. D. D. Fang, Y. Z. Pei, Y. F. Lv, L. S. Chen, Periodicity induced by state feedback controls and driven by disparate dynamics of a herbivore-plankton model with cannibalism, *Nonlinear Dyn.*, **90** (2017), 2657–2672. https://doi.org/10.1007/s11071-017-3829-y

23. D. Z. Li, Y. Liu, H. D. Cheng, Dynamic complexity of a phytoplankton-fish model with the impulsive feedback control by means of poincare map, *Complexity*, **2020** (2020), 8974763. https://doi.org/10.1155/2020/8974763

24. J. Yang, S. Y. Tang, Holling type II predator-prey model with nonlinear pulse as state-dependent feedback control, *J. Comput. Appl. Math.*, **291** (2016), 225–241. https://doi.org/10.1016/j.cam.2015.01.017

25. Z. Z. Shi, H. D. Cheng, Y. Liu, Y. H. Wang, Optimization of an integrated feedback control for a pest management predator-prey model, *Math. Biosci. Eng.*, **16** (2019), 7963–7981. https://doi.org/10.3934/mbe.2019401

26. I. U. Khan, S. Y. Tang, The impulsive model with pest density and its change rate dependent feedback control, *Discrete Dyn. Nat. Soc.*, **2020** (2020), 4561241. https://doi.org/10.1155/2020/4561241

27. T. T. Li, W. C. Zhao, Periodic solution of a neutral delay leslie predator-prey model and the effect of random perturbation on the smith growth model, *Complexity*, **2020** (2020), 8428269. https://doi.org/10.1155/2020/8428269

28. Y. N. Li, Y. Li, Y. Liu, H. D. Cheng, Stability analysis and control optimization of a prey-predator model with linear feedback control, *Discrete Dyn. Nat. Soc.*, **2018** (2018), 4945728. https://doi.org/10.1155/2018/4945728

29. H. J. Guo, L. S. Chen, X. Y. Song, Qualitative analysis of impulsive state feedback control to an algae-fish system with bistable property, *Appl. Math. Comput.*, **271** (2015), 905–922. https://doi.org/10.1016/j.amc.2015.09.046

30. Q. Q. Zhang, S. Y. Tang, Bifurcation analysis of an ecological model with nonlinear state–dependent feedback control by poincaré map defined in phase set, *Commun. Nonlinear Sci.*, **108** (2022), 106212. https://doi.org/10.1016/j.cnsns.2021.106212

31. Y. Z. Wu, G. Y. Tang, C. C. Xiang, Dynamic analysis of a predator-prey state-dependent impulsive model with fear effect in which action threshold depending on the prey density and its changing rate, *Math. Biosci. Eng.*, **19** (2022), 13152–13171. https://doi.org/10.3934/mbe.2022615

32. Y. Tian, Y. Gao, K. B. Sun, Global dynamics analysis of instantaneous harvest fishery model guided by weighted escapement strategy, *Chaos Solitons Fract.*, **164** (2022), 112597. https://doi.org/10.1016/j.chaos.2022.112597

33. I. U. Khan, S. Y. Tang, B. Tang, The state-dependent impulsive model with action threshold depending on the pest density and its changing rate, *Complexity*, **2019** (2019), 6509867. https://doi.org/10.1155/2019/6509867

34. G. Wang, M. Yi, S. Y. Tang, Dynamics of an antitumour model with pulsed radioimmunotherapy, *Comput. Math. Methods Med.*, **2022** (2022), 4692772. https://doi.org/10.1155/2022/4692772

35. W. Li, T. H. Zhang, Y. F. Wang, H. D. Cheng, Dynamic analysis of a plankton-herbivore state-dependent impulsive model with action threshold depending on the density and its changing rate, *Nonlinear Dyn.*, **107** (2022), 2951–2963. https://doi.org/10.1007/s11071-021-07022-w

36. B. Tang, W. Q. Zhao, Sliding dynamics and bifurcations of a filippov system with nonlinear threshold control, *Int. J. Bifurcat. Chaos*, **31** (2021), 2150214. https://doi.org/10.1142/S021812742150214X

37. Y. F. Li, S. Huang, X. Y. Song, Global dynamic analysis of a nonlinear state-dependent feedback control SIR model with saturation incidence, *Eur. Phys. J. Plus*, **138** (2023), 636. https://doi.org/10.1140/epjp/s13360-023-04277-7

38. T. Y. Cheng, S. Y. Tang, R. A. Cheke, Threshold dynamics and bifurcation of a state-dependent feedback nonlinear control susceptible-infected-recovered model, *J. Comput. Nonlinear Dyn.*, **14** (2019), 071001. https://doi.org/10.1115/1.4043001

39. Q. Q. Zhang, B. Tang, S. Y. Tang, Vaccination threshold size and backward bifurcation of SIR model with state-dependent pulse control, *J. Theor. Biol.*, **455** (2018), 75–85. https://doi.org/10.1016/j.jtbi.2018.07.010

40. R. J. Smith, E. J. Schwartz, Predicting the potential impact of a cytotoxic T-lymphocyte HIV vaccine: How often should you vaccinate and how strong should the vaccine be? *Math. Biosci.*, **212** (2008), 180–187. https://doi.org/10.1016/j.mbs.2008.02.001

41. B. Tang, Y. N. Xiao, S. Y. Tang, R. A. Cheke, A feedback control model of comprehensive therapy for treating immunogenic tumours, *Int. J. Bifurcat. Chaos*, **26** (2016), 1650039. https://doi.org/10.1142/S0218127416500395

42. Z. Q. Liang, G. P. Pang, X. P. Zeng, Y. H. Liang, Qualitative analysis of a predator-prey system with mutual interference and impulsive state feedback control, *Nonlinear Dyn.*, **87** (2017), 1495–1509. https://doi.org/10.1007/s11071-016-3129-y

AIMS Press